

J.-S. von Storch · P. Müller · E. Bauer

# Climate variability in millennium integrations with coupled atmosphere-ocean GCMs: a spectral view

Received: 12 January 2000 / Accepted: 14 June 2000

**Abstract** Climate variations in four millennium integrations obtained with coupled GCMs are studied from a spectral point of view. It is shown that the bulk of these variations can be described by two distinctly different types of spectra. The type-I spectra, characterized by a high-frequency  $\omega^{-2}$  slope (with  $\omega$  being frequency) and a low-frequency plateau, indicate the dominance of short-term fluctuations in generating climate variations. They are obtained for many atmospheric variables and variables representing predominantly the upper ocean and the high-latitude part of the deep ocean. The time scale, at which the spectra level off, varies from a few days for grid-point time series of atmospheric variables, to a few months for time series of large-scale atmospheric patterns, several years for SST anomalies in the tropical Pacific, and a few decades for variables describing oceanic baroclinic waves. The type-II spectra are obtained in the ocean interior, which is shielded from the fluctuating forcing at the surface. Since the ocean model does not produce oceanic eddies, the disappearance of type-I spectra in the deep ocean indicates that the fluctuating surface forcing does not fully penetrate into the deep ocean. While type-I spectra are supported by observations, type-II spectra might describe a model specific phenomenon and the realism of these spectra is still a open question.

---

J.-S. von Storch (✉)  
Meteorologisches Institut, Universität Hamburg  
Hamburg, Germany

P. Müller  
Department of Oceanography,  
University of Hawaii, Honolulu, Hawaii

E. Bauer  
Potsdam Institut for Climate Impact Research,  
Potsdam, Germany

*Present address:*  
J.-S. von Storch  
Institute of Hydrophysics, GKSS Research Center,  
21502 Geesthacht, Germany  
E-mail: jin@gkss.de

---

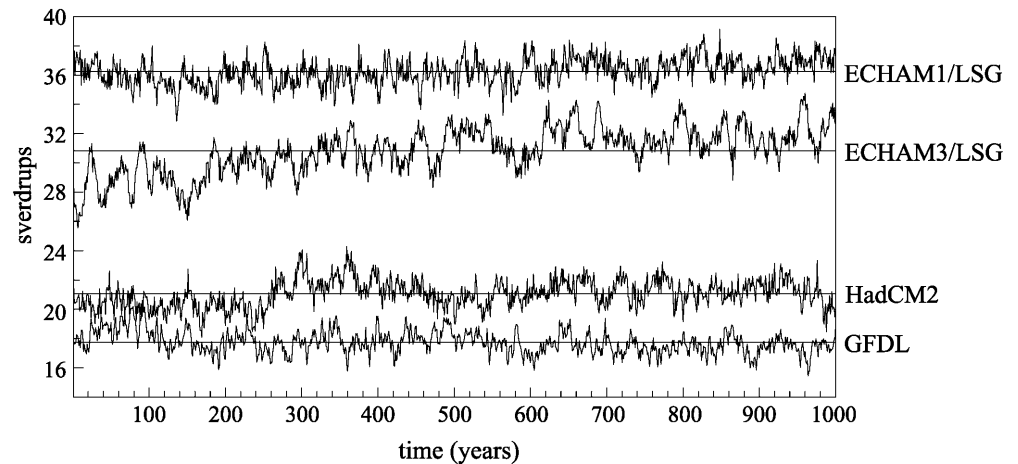
## 1 Introduction

In recent years, several integrations over time periods of more than one thousand years have been performed using coupled atmosphere-ocean general circulation models (GCMs) (Manabe and Stouffer 1996; Tett et al. 1997; Voss et al. 1998; von Storch et al. 1997). These long integrations form a new basis for studying climate variability. In particular, it is possible to obtain, within the framework of coupled GCMs, a complete description of climate variability on a broad range of time scales. Even though the variability in these millennium integrations cannot be expected to be completely realistic, such a description is a necessary first step towards the improvement of our understanding of the climate system.

The most intuitive way to describe climate variability is to consider time series of climate variables. A few examples are given in Fig. 1, which shows time series of the mean annual northward mass transport in the Atlantic which characterizes the overturning in the Atlantic. The time series are derived from four 1000-year integrations with different coupled GCMs (von Storch et al. 2000). They show some episodes marked by large amplitudes which persist over a time period of a decade or longer, indicating the existence of variability on long time scales. However, the time series shown also vary on other time scales. In general, they are irregular in time. A given segment of a time series never exactly repeats itself during the 1000-year time interval considered, even when it is produced by the same model. The irregularity becomes more severe when considering atmospheric time series.

Because of the irregularities, the consideration of an individual event, e.g. defined as large positive values occurring persistently during a certain time interval at a certain location, cannot provide conclusive statements about the variability. A statistical description is required instead. Such a description concerns “averaged” quantities, such as variances and covariances, or their

**Fig. 1** Time series of maximal overturning in the Atlantic (in Sverdrups), as obtained from four integrations with coupled GCMs (von Storch et al. 1999). The maximal overturning is defined as the maximum of the positive stream function. It characterizes the northward mass transport in the Atlantic. The horizontal lines indicate the 1000-year averages



frequency decompositions, i.e. spectra and cross spectra. In this work, the modelled variations are studied in terms of spectra.

Spectral features of variations in millennium integrations have been considered separately for different components of the modelled climate system. Stouffer et al. (2000) studied the spectra of surface air temperature in three 1000-year coupled atmosphere-ocean GCMs. The spectral features of the large-scale atmospheric variations in the coupled ECHAM1/LSG model were studied by von Storch (1994, 1999). Spectral features related to baroclinic Rossby waves in the upper ocean in the same integration were investigated by Frankignoul et al. (1997). The spectral behaviour of the deep-ocean mass-transport in four different millennium integrations was analyzed in von Storch et al. (2000). The purpose here is to summarize these results. It will be shown that variations of various climate variables in the millennium integrations can be summarized in terms of two distinct types of spectra.

Section 2 gives a short introduction to coupled GCMs used for millennium integrations. The introduction provides not only a brief overview of the models, it also emphasizes potential problems of these models when used in the millennium integrations. The time-mean states produced by these models are described in Sect. 3. The two types of climate variability found in the millennium integrations are discussed in Sect. 4. A large portion of the results is derived from the 1260-year integration with the coupled ECHAM1/LSG model of the Max Planck Institut (Hamburg, Germany) (von Storch et al. 1997). Some conclusions concerning the variability of the deep ocean are drawn from the 1000-year integrations (von Storch et al. 2000) performed at the Geophysical Fluid Dynamics Laboratory (Princeton, USA), the German Climate Computer Center (Hamburg, Germany) and the Hadley Centre (Bracknell, UK). The run of the German Climate Computer Center is carried out using the same ocean GCM, but a different version of the atmospheric GCM and a different spin-up procedure. The three additional integrations will be referred to as the GFDL, ECHAM3/LSG and HadCM2

runs, respectively. Discussions and conclusions are given in the last two sections.

## 2 Model description

The coupled GCMs comprise two major components. One represents the atmosphere and the other the ocean. They are formulated based on the conservation principles of momentum, heat and mass (not only for the total air/water mass, but also for its components such as moisture in the atmosphere and salt in the ocean). The two models are coupled to each other through fluxes of momentum, heat and fresh water at the interface between the atmosphere and the ocean. The millennium integrations considered are obtained by running the coupled models without external forcings, like those related to solar activities or to changes in CO<sub>2</sub> concentration. Although all coupled GCMs are based on the same first principles, some features, such as resolution, parametrizations of subgrid processes and the representations of processes not included in the atmosphere and ocean models (e.g. sea ice), can differ from GCM to GCM. In the following, some properties are considered which are common to the coupled GCMs used for the millennium integrations. Possible implications for the simulated variability are discussed. The issues considered may give some hints about how realistic the model variability is. However, the question of realism is not systematically pursued here.

### 2.1 Resolutions and their implication for the variability

Due to limited computer capacity, the coupled GCMs used for the millennium integrations have generally coarse resolutions. The atmospheric component of the GFDL model uses a spectral representation with a R15 rhomboidal truncation. A predicted variable is represented using 15 zonal waves and 15 associated Legendre functions. The oceanic component has a meridional resolution of 4.5° and a zonal resolution of 3.7°. In the case of the two ECHAM/LSG models, the atmospheric model (the ECHAM model) is based on a spectral representation with a triangular truncation at a total wave number of 21. The ocean model (the LSG model) has an effective horizontal grid size of 4° by 4°. The HadCM2 coupled model has the finest resolution. Different from the ECHAM and the GFDL model, the atmospheric component of the HadCM2 is a grid-point model. The oceanic component has a meridional resolution of 2.5° and a zonal resolution of 3.75°, and its atmospheric component has a congruent grid.

For all models considered, the resolutions are too coarse to resolve oceanic eddies, but fine enough to resolve, at least partly, atmospheric eddies, which contributes to the bulk of atmospheric

variations. Consequently, the oceanic circulation produced by the ocean-only models (driven by climatological fluxes) is, to a large extent, laminar, whereas the atmospheric circulation produced by atmosphere-only models (driven by climatological SST) is turbulent. The picture of a steady and laminar flow obtained from coarse-resolution ocean-only models contributes to the oversimplified picture of a “global conveyor belt”. The oceanic flow can, however, become turbulent when it is obtained by coupling a coarse-resolution ocean model to a turbulent atmosphere. The bulk of oceanic variations are then generated by the fluctuating fluxes at the surface. All millennium integrations considered are obtained by coupling an eddy resolving atmospheric model to a non-eddy resolving oceanic model. In such coupled integrations, the atmospheric variations are (apart from those resulting from interactions with SST) essentially internally generated, whereas the oceanic variations are essentially externally forced.

## 2.2 Parametrizations

Subscale processes are represented through parametrizations. Unfortunately, the parametrizations in the models considered are tuned to reproduce the observed time-mean state. The extent to which these parametrizations appropriately represent the effect of the subgrid processes on the variability is not known and has not yet been studied systematically. In addition, the ECHAM1/LSG model is not equipped with the most recently developed parametrization package, nor are the other coupled GCMs, e.g. the coupled GCM used at the Geophysical Fluid Dynamics Laboratory in Princeton (USA) (Manabe et al. 1991).

There are also processes not represented in the atmosphere and ocean GCMs, but which are important for the climate system. An example is the glacier dynamics including the calving of glaciers. The neglect of glacier dynamics may lead to problems in the hydrological cycle. These problems become particularly apparent, e.g. in terms of salinity trends, when the models are integrated over one thousand years (von Storch et al. 1997). To what extent these problems affect the variability is unknown.

## 2.3 Coupling with flux corrections

The time-mean surface fluxes produced by the coupled models are generally not identical to those used to drive the uncoupled models. Thus, when the two models are coupled together, the coupled system tends to reach an equilibrium state different from the desired climate state, a phenomenon known as climate drift.

In order to avoid climate drift, flux corrections accounting for the differences between the simulated and the observed time-mean fluxes are applied (Sausen et al. 1988). All coupled models considered are flux corrected. The implementation of flux corrections is equivalent to coupling the atmosphere and the ocean with anomalies of the fluxes computed relative to the equilibrium states of the two uncoupled sub-systems.

## 2.4 Spin-up of the deep ocean

The procedure to bring a system to its equilibrium state is called spin-up. In contrast to the atmosphere, which can be spun up within a few years, the time required for the deep ocean to reach its equilibrium is of the order of  $10^3$  to  $10^4$  years. In order to reduce the computational expense, the deep ocean is therefore normally first spun up in an uncoupled mode over a long time period using prescribed surface fluxes (Cubasch et al. 1992; Manabe et al. 1991; Voss 1996). When then coupled to the atmosphere, the deep ocean may experience a shock. As an alternative, coupled spin-up of the deep ocean, designed to avoid the coupling shock, is used in the HadCM2 integration. However, due to the high computational costs, the coupled spin-up is much shorter. It is possible that different spin-up runs lead to different mean states and different variability in the deep ocean. However, such a possibility cannot be further quantified so far.

Apart from the techniques used in the GFDL, HadCM2 and ECHAM/LSG models, there are also other ways to avoid the climate drift and coupling shock (Stouffer and Dixon 1998). In general, there is a long way to go to obtain long-term integrations which realistically describe variations in the climate system. The first step in this direction is to characterize the variations captured by the state-of-art millennium integrations, and to understand whether these variations are consequences of the problems addressed. These issues will be revisited in Sect. 5.

## 3 Time-mean state

The large-scale features of the time-mean circulation in the millennium integrations considered here are consistent with the observational evidence. Two examples, concerning the simulated time-mean states of the atmosphere and the ocean, are considered.

The first example gives some hint about the time-mean state of the atmosphere simulated by the ECHAM1/LSG model. Figure 2 shows the distribution of sea level pressure (SLP) in northern winter (December–February) and in northern summer (June–August) averaged over the last 810 years. For comparison, the climatological distribution of SLP based on the 1986–95 ECMWF analysis is also shown. The Aleutian low during DJF in the model is about 5 hPa deeper than in the observations. The Iceland low is underestimated and shifted about  $20^\circ$  southwards relative to the observed one, causing a southward shift of the Atlantic gyre system. The mean SLP values over the Arctic are up to 15 hPa overestimated during northern winter. In northern summer, the model reproduces the observed surface pressure relatively well, with slightly underestimated high pressure systems over the northern oceans.

In the Southern Hemisphere the sub-tropical highs are about 5 hPa weaker than observed in both seasons and the sub-polar lows around Antarctica are 10–20 hPa weaker than in the observations. As a result, the meridional pressure gradient in the latitude band  $30$ – $50^\circ$ S is strongly underestimated in the model compared to the present climate. Another feature which is evident in both the ECHAM1/LSG model and some other low resolution uncoupled atmospheric models (Xu et al. 1990) is that the values of SLP are too high over Antarctica.

Despite the differences between the simulated and the observed distributions, Fig. 2 suggests that the dominant large-scale features of the time-mean SLP fields, i.e. the distribution of highs and lows, are captured by the ECHAM1/LSG model.

The second example of the simulated time-mean circulation is given in Fig. 3, which shows the 1000-year means of the zonally averaged stream functions in the vertical-meridional section of the Atlantic, as obtained from the GFDL, ECHAM3/LSG, ECHAM1/LSG and HadCM2 integrations.

Although the strength and the location of the circulation differ from integration to integration (see also Fig. 1), the gross features of the Atlantic overturning, i.e. northward inflow in the upper 1000 to 2000 m, the subsequent deep-water formation in the North Atlantic

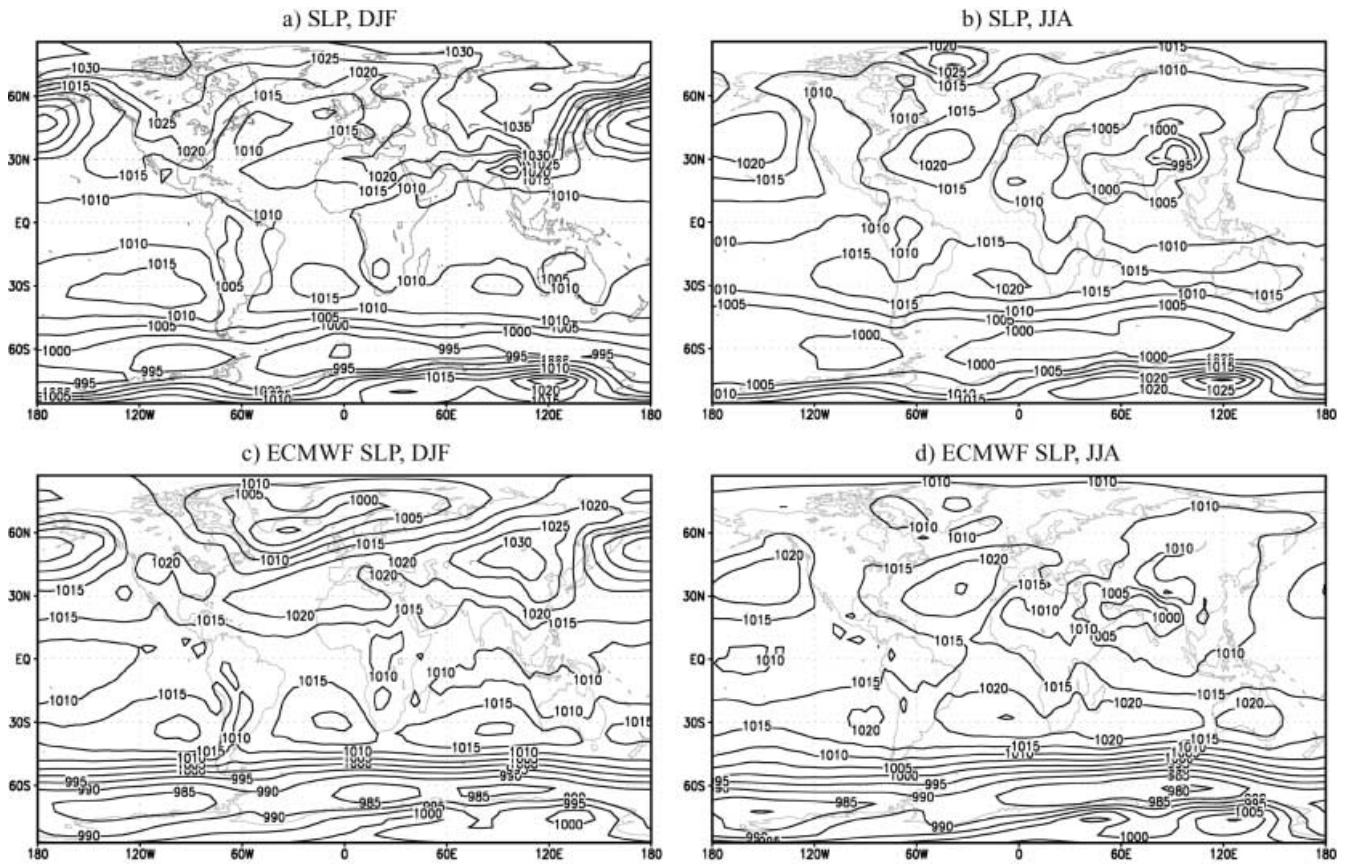


**Fig. 2a–d** Mean sea level pressure in **a** northern winter DJF and **b** in northern summer JJA averaged over the last 810 years of the ECHAM1/LSG run. For comparison, climatological distributions

based on the ECMWF analysis from 1986 to 1995 are shown in **(c** DJF) and **(d** JJA). Contour interval is 5 hPa

and southward spreading in the deep Atlantic, and Antarctic inflow from still deeper layers, are produced by all models. Using observational data in the Atlantic, Roemmich and Wunsch (1985) estimated that  $17 \pm 4$  Sverdrups of relatively warm thermocline and intermediate water flow northwards at  $24^\circ\text{N}$ ; and below this  $20 \pm 5$  Sverdrups, identified as North Atlantic Deep Water (NADW), flow southwards. Further below, about  $3 \pm 3$  Sverdrups of Antarctic Bottom Water (AABW) flow northwards. Figure 3 suggests that the transport of the NADW in the GFDL and the HadCM2 runs is close to the lower bound of the estimates of Roemmich and Wunsch (1985) and that in the two ECHAM/LSG runs it is close to or above the upper bound of these estimates. The transport of northward AABW is underestimated in ECHAM1/LSG. The numbers produced by the ECHAM3/LSG run are more comparable to the values of Roemmich and Wunsch (1985) than those produced by the ECHAM1/LSG run.

#### 4 Two types of climate variations

The variations around the time-mean state can be described predominantly by two types of frequency spectra. The properties and the distributions of these spectra

are investigated in this section. All spectra are represented in log-log plots. Denoting frequency by  $\omega$ , a spectral power law  $c\omega^{-\beta}$  appears as a straight line in the log-log plot.  $\beta = 0$  corresponds to a white spectrum, and  $\beta > 1$  ( $\beta < 1$ ) indicates that the spectrum increases (decreases) with decreasing frequency. In the following,  $\beta$  derived from atmospheric and oceanic variables are denoted by superscripts  $a$  and  $o$ . In order to distinguish  $\beta$  at low and high frequencies, subscripts  $h$  and  $l$  are also used.

For time series which resolve the annual cycle (i.e. monthly or daily time series), spectra are estimated from anomaly time series obtained by removing the corresponding climatological annual cycle.

##### 4.1 Type I

The first type of spectra, as sketched at the top of Fig. 4, is characterized by a spectral slope at high frequencies and a flat spectrum at low frequencies. The slope indicates an increase of spectral energy with decreasing frequency at high frequencies. For large-scale atmospheric variations and some variations in the ocean the high-frequency slope  $\beta_h$  is close to two. When grid-point atmospheric time series are considered, larger values of

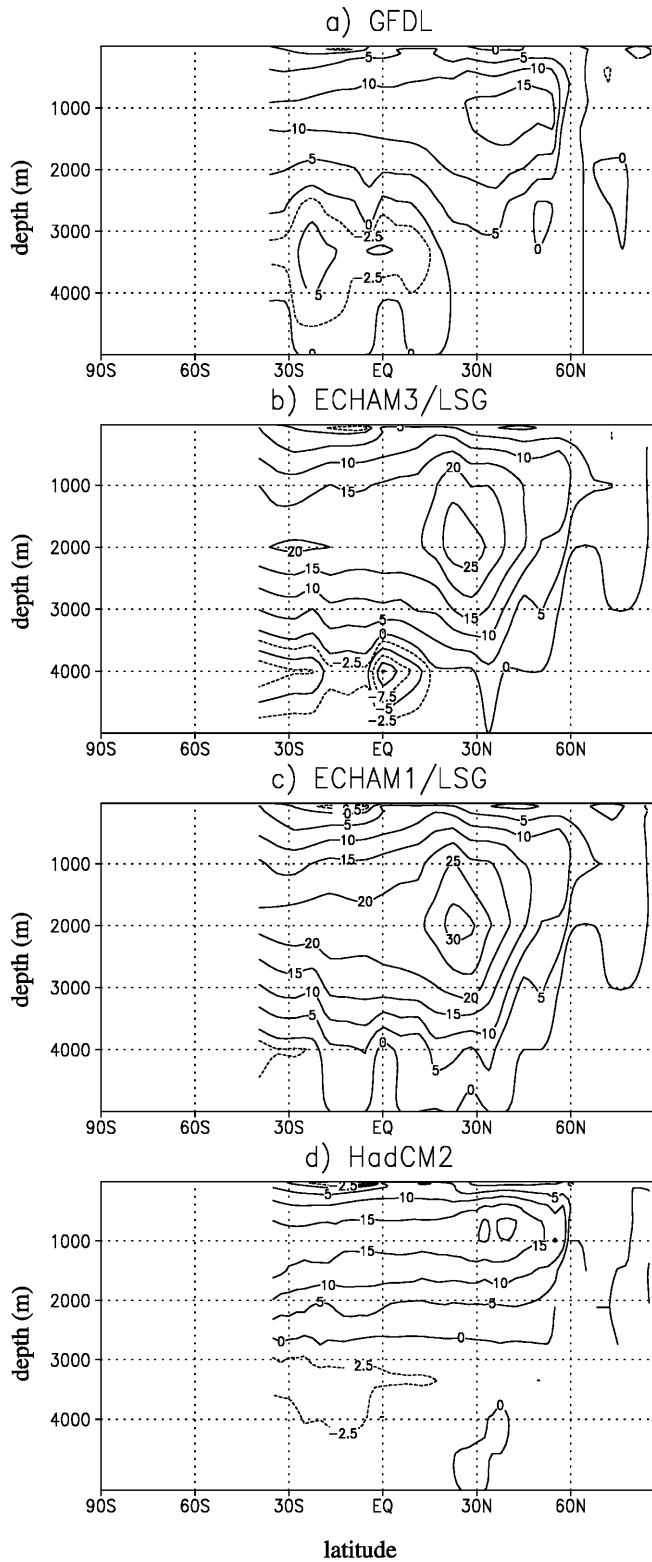


**Fig. 3a–d** The 1000-year means of vertical-meridional sections of zonally averaged stream functions derived from the integrations with the coupled GFDL, ECHAM3 /LSG, ECHAM1/LSG and HadCM2 models. Intervals of *solid isolines* are 5 Sverdrups. For the negative stream functions in the Atlantic, additional isolines are plotted every 2.5 Sverdrups

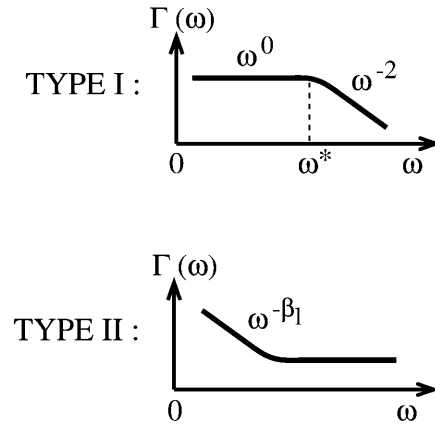


**Fig. 4** Schematic diagrams of the two types of spectra found in the millennium integrations. Type-I spectra are characteristic for many atmospheric variables and variables representing predominantly the upper ocean and the high-latitude part of the deep ocean. Type-II spectra are characteristic for variations in the tropical and subtropical oceans which are shielded from short-term fluctuations originating from the atmosphere

$\beta_h^a$  are found at extremely high frequencies. The time scale at which the spectrum turns flat is  $\tau^* = 1/\omega^*$ . The flatness at low frequencies indicates that the variability is essentially white on time scales longer than  $\tau^*$ . The time scale  $\tau^*$  varies from a few days to a few decades, depending on the variable considered. The extent to which the type-I spectrum is typical for variations in the ECHAM1/LSG integration is considered next.

#### 4.1.1 Spectra of daily grid-point time series in the atmosphere

An example of a spectrum of a grid-point time series is shown in Fig. 5a. It is derived from the ECHAM1/LSG integration using 100 years of daily surface pressure at the grid point near Potsdam (Germany). This time series is chosen since observed pressure data over a long time period are available from the Potsdam station. The corresponding spectrum at this station is shown in Fig. 5b. Since a model grid point represents a large area, small-scale features (in both time and space) which show up in the station data could not be modelled. The comparison of Fig. 5a with Fig. 5b should indicate how these small-scale features affect the overall spectral behaviour.

The low-frequency shapes of the modelled and observed spectra are comparable, although the model underestimates the overall pressure variability. Both show a flat spectral plateau at low frequencies and are proportional to  $\omega^{-2}$  over the high-frequency range [ $0.1 < \omega < 0.4$ ] cpd (cycles per day). A discrepancy is found at extremely high frequencies with  $\omega > 0.4$ , corresponding to time scales shorter than 2.5 days. At these frequencies, the modelled spectrum tends to have a steeper slope than the observed one. The similarities at low frequencies and the discrepancy at extremely high

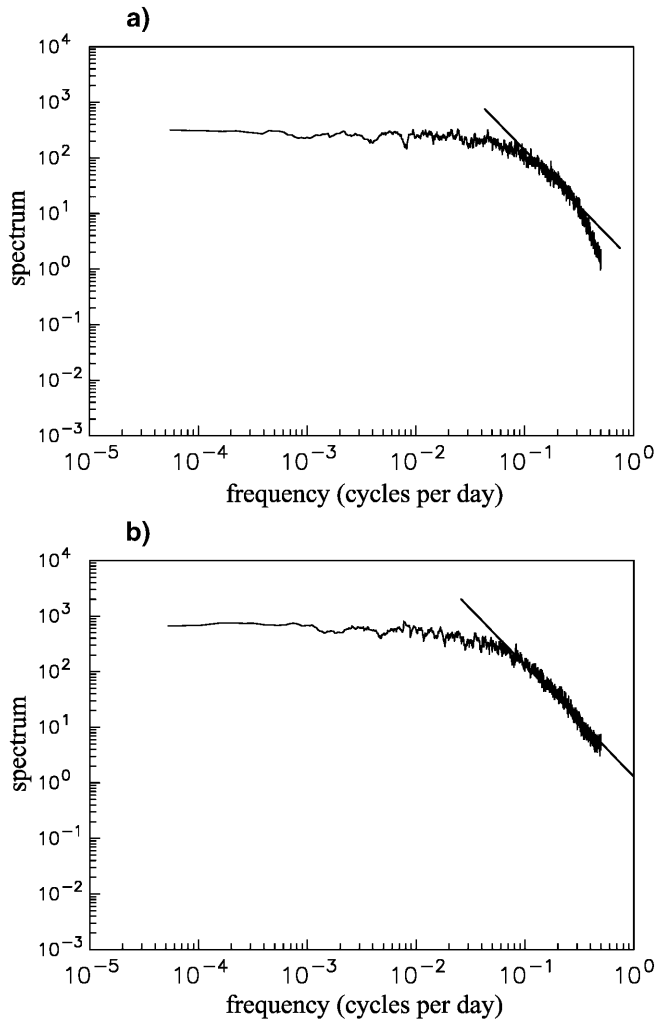


**Fig. 5a, b** Spectrum of daily surface pressure at (52°N, 13°E) (*top panel*). The spectrum is first derived from two consecutive chunks, and then smoothed using running averages with the averaging interval being 21. For comparison, the spectrum estimated in the same manner from surface pressure at the nearby Potsdam station is shown at the *bottom*. Frequency is in cycles per day

frequencies between the modelled and observed spectra are also found at other grid points (not shown), indicating that the unresolved small-scale features significantly affect the high-frequency spectral behaviour of the resolved variable, but have little influence on the overall low-frequency spectral shape.

In the following we discuss the extent to which the low-frequency plateau and the high-frequency  $\omega^{-2}$  slope can be identified for grid-point time series in the ECHAM1/LSG integration. This is done by fitting the power law  $c\omega^{-\beta^a}$  to the low-frequency ( $\omega < 0.01$  cpd) and high-frequency ( $0.1 < \omega < 0.4$  cpd) parts of the spectra of the zonal velocity at 200 and 900 hPa.

The high-frequency power  $\beta_h^a$  (Fig. 6) shows smaller spatial variations at 200 hPa than at 900 hPa. At 200 hPa, apart from some polar regions,  $\beta_h^a$  is between 1.5 and 2.5. At 900 hPa, there are two large areas where  $\beta_h^a$  is larger than 2.5. One is in the tropical Indian Ocean

and the tropical western Pacific and the other is over the Arctic and northern Europe. Small values of  $\beta_h^a$  are found over the North Pacific. Apart from these regions,  $\beta_h^a$  is between 1.5 and 2.5.

Independent of the exact values of  $\beta_h^a$ , the low-frequency slope  $\beta_l^a$  is uniform in both the lower and upper troposphere, as indicated by the grey area in Fig. 7, where the value of  $\beta_l^a$  is between 0.5 and  $-0.5$ . A similar picture is also obtained for the meridional velocity (not shown). The result suggests that the grid-point time series in the ECHAM1/LSG atmosphere are white on time scales longer than 100 days.

Note that type-I spectra with  $\beta_h = 2$  can be obtained from a first-order auto-regressive [AR(1)] process. An AR(1) process is characterized by the process parameter  $\alpha$  (which is the lag-1 correlation of the process). One can estimate the time scale  $\tau^*$  from  $\alpha$ . Let  $\Gamma_n$  be the spectrum of the driving white noise forcing of the AR(1) process. The spectrum  $\Gamma$  of the AR(1) process (see e.g. von Storch and Zwiers 1999) is then given by

$$\Gamma(\omega) = \frac{\Gamma_n(\omega)}{1 - 2\alpha \cos(2\pi\omega) + \alpha^2}$$

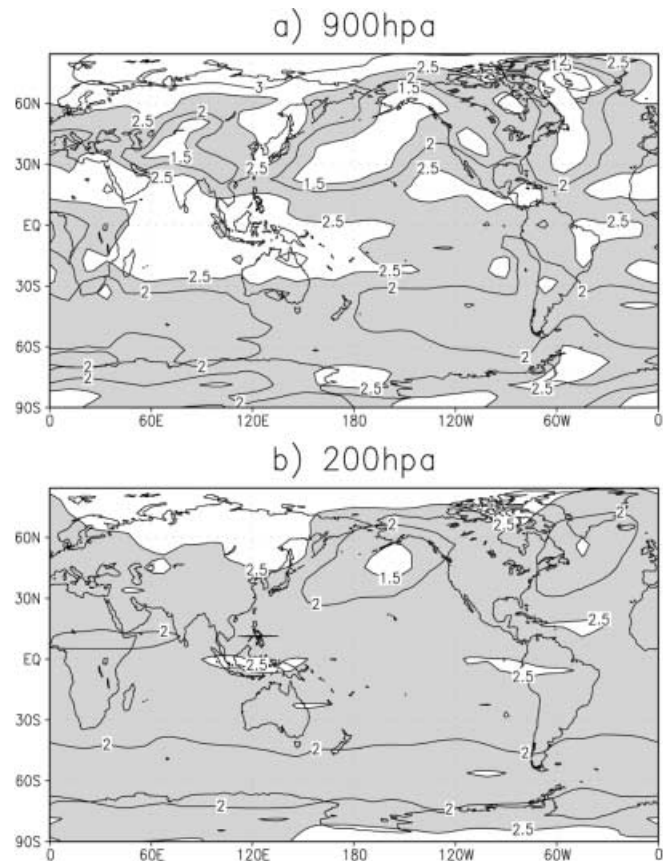


**Fig. 6a, b** High-frequency spectral power  $\beta_h^a$  of daily zonal velocity at 900 (*top*) and 200 (*bottom*) hPa, obtained from 100 years of the ECHAM1/LSG integration. The *grey areas* indicate the areas where values of the spectral power  $\beta_h^a$  are about two (i.e.  $1.5 < \beta_h^a < 2.5$ ). The power  $\beta_h^a$  is obtained by fitting a power law  $c\omega^{-\beta_h^a}$  to the interval extending from 0.1 to 0.4 cycles per day

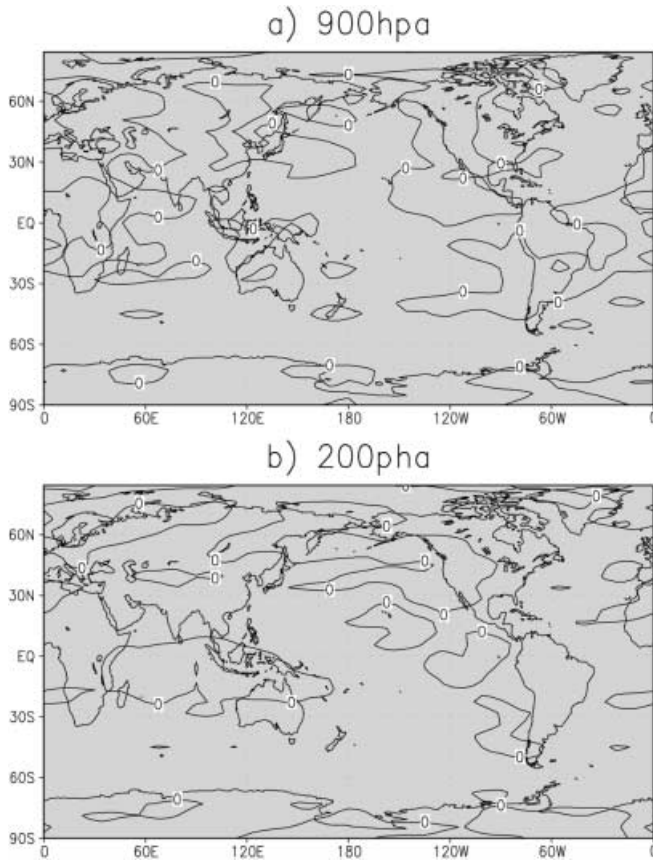


**Fig. 7a, b** Low-frequency spectral power  $\beta_l^a$  of daily zonal velocity at 900 (top) and 200 (bottom) hPa, obtained from 100 years of the ECHAM1/LSG integration. The grey areas indicate the areas where values of the spectral power  $\beta_l^a$  are about zero (i.e.  $-0.5 < \beta_l^a < 0.5$ ). The power  $\beta_l^a$  is obtained by fitting a power law  $c\omega^{-\beta_l^a}$  to the frequency range  $\omega < 0.01$  cycles per day

where  $\omega \in [0, 0.5]$ . For  $\omega \ll 1/(2\pi)$ , it reduces to

$$\Gamma(\omega) = \frac{\Gamma_n(\omega)}{(1 - \alpha)^2 + \alpha(2\pi\omega)^2}$$

For white noise forcing,  $\Gamma_n(\omega)$  is constant. The shape of the spectrum is thus characterized at high and low frequencies by

$$\Gamma(\omega) \propto \begin{cases} [1/(\alpha(2\pi)^2)]\omega^{-2} & \text{for } \omega \gg \omega^* \\ 1/(1 - \alpha)^2 & \text{for } \omega \ll \omega^* \end{cases} \quad (1)$$

where  $\omega^* = 1/\tau^* = (1 - \alpha)/(2\pi\alpha^{1/2})$ . Figure 7 suggests that  $\tau^*$  is no longer than 100 days for daily grid-point time series of atmospheric variables.

#### 4.1.2 Spectra of large-scale atmospheric patterns

Large-scale variations can be described by large-scale patterns and their corresponding time series. In the following, such patterns are obtained from EOF-analyses (empirical orthogonal function analysis) of global anomaly fields of various variables. Figure 8 shows the spectra of the first two PCs of the 200-hPa stream

function, which are derived from 200-year of daily PCs (obtained by projecting the daily data onto the EOF patterns of monthly data). The spectra are comparable to the top panel in Fig. 4 with the high-frequency slope being close to 2. The time scale  $\tau^*$  at which the spectra become flat are of the order of a few months.

The time scale  $\tau^*$  of large-scale atmospheric variations in the ECHAM1/LSG model was estimated by von Storch (1999) by fitting an AR(1) process to the PC time series. The analysis was concentrated on the stream function and the velocity potential, which completely describe horizontal motions. In order to additionally capture vertical variations, the stream function and velocity potential at 200, 500 and 850 hPa are considered. The EOFs were calculated from 500-year monthly unfiltered anomaly fields.

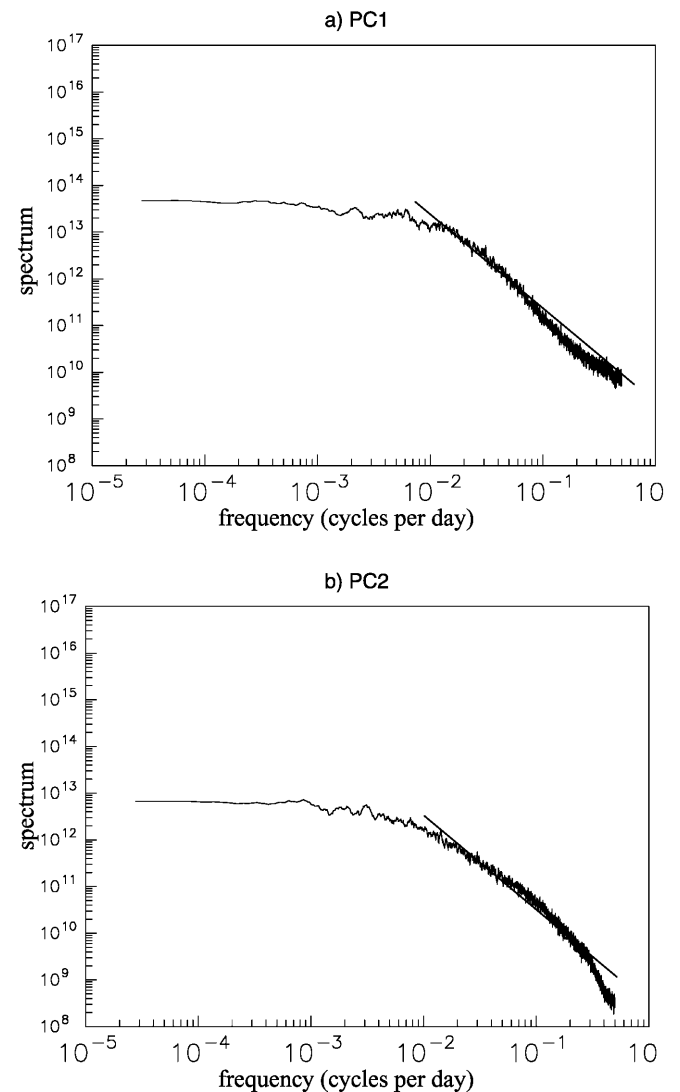


**Fig. 8a, b** Spectra of daily time series of the first two EOFs derived from the 200-hPa stream function of the ECHAM1/LSG integration. The spectrum is first derived from two consecutive chunks, and then smoothed using running averages with the averaging interval being 21. The frequency is in cycles per day

The time scales  $\tau^* = 1/\omega^*$  of the first 10 leading PCs for the stream function and velocity potential at the chosen levels are shown in Fig. 9. For velocity potential, the only large value is obtained from the sixth PC at 850 hPa. The corresponding EOF pattern (not shown) shows large anomalies near Antarctica, indicating that this mode is related to the initial drift of the sea ice during the coupled integration (von Storch et al. 1997). Apart from this value,  $\tau^*$  of the stream function (Fig. 9b) is noticeably larger than that of the velocity potential (Fig. 9a), suggesting that the non-divergent flow is redder than the non-rotational flow. The largest  $\tau^*$  values, up to about 11 months, result from the first two PCs of the stream function. Thus, for the large-scale atmospheric variations in the ECHAM1/LSG integration, the time scale  $\tau^*$  is about a few months up to a year, which is much longer than that for grid point time series.

4.1.3 Spectra of ENSO-related monthly time series

Timmermann and Latif (1999) showed that the ECHAM3/LSG model produced ENSO-type variations.

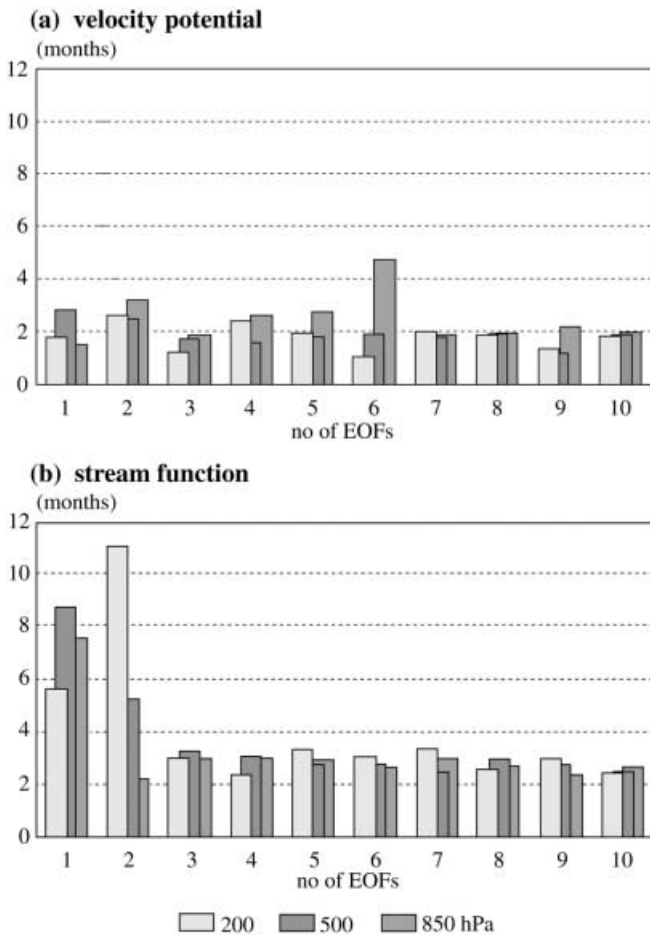


Fig. 9a, b The time scale  $\tau^*$  (in months) as functions of the orders of the EOFs obtained from the atmosphere of the ECHAM1/LSG model. The values of  $\tau^*$  are derived from the PCs of a the velocity potential and b the stream function at 200, 500 and 850 hPa

Consistent with their results, Fig. 10 shows that the spectrum of NINO3 SST (averaged SST in the region extending from 5°S to 5°N and from 100°W to 140°W) derived from the 1000-year integration with the ECHAM3/LSG model is comparable to that derived from the GISST (Global Ice and Sea Surface Temperature) data set for the period 1903 to 1994. The ECHAM3/LSG model underestimates variations in the SST time series. However, the underestimation occurs on all time scales so that the overall spectral shape is essentially reproduced by the model. For both the observed and modelled spectra, the high-frequency slope is close to  $\omega^{-2}$  and a plateau is found at low frequencies. The most pronounced difference between the observed and modelled spectra may be the frequency  $\omega^* = 1/\tau^*$ , at which the spectra level off. It is near 0.02–0.03 cpm (cycles per month), i.e. around 3 to 4 years, in the observation, but close to 0.01 cpm, i.e. around 7 to 8 years, in the model.

The ENSO-related atmospheric variations on inter-annual time scales are strongly underestimated in the ECHAM3/LSG integration. The underestimation may be a consequence of the fact that the atmosphere is forced by too weak SST variations. When considering the pressure difference between grid points close to Darwin and Tahiti, one finds a spectrum which is white on interannual time scales, consistent with Sects. 4.1.1 and 4.1.2.

Figures 9 and 10 indicate that the time scale  $\tau^*$  of NINO3 SST is much longer than  $\tau^*$  of an atmospheric variable. This change becomes more pronounced when

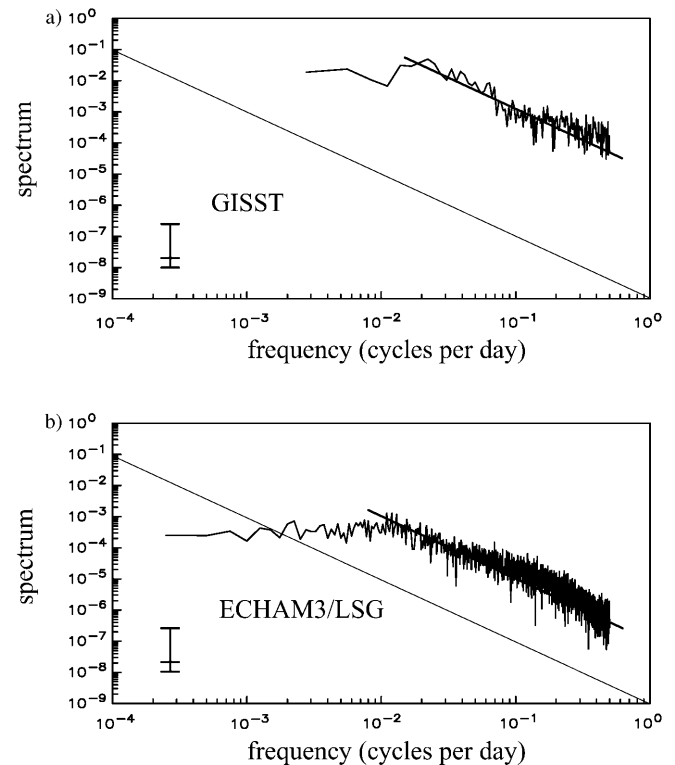


Fig. 10a, b Spectra of NINO3-SST time series, as estimated from the GISST time series extending from 1903 to 1994 (top) and from the millennium integration with the ECHAM3/LSG model (bottom). Frequency is in cycles per month

considering variability related to oceanic baroclinic waves.

#### 4.1.4 Spectra of yearly time series related to baroclinic Rossby waves

Frankignoul et al. (1997) constructed a simple linear model of the extratropical baroclinic Rossby waves driven by stochastic wind stress forcing. The baroclinic spectra predicted by the model were then compared with the North Atlantic pressure variability in the ECHAM1/LSG millennium integration. Figure 11 shows spectra of the ECHAM1/LSG baroclinic pressure at 250 m and 30°N for various longitudes in the Atlantic. The spectra are red with a high-frequency  $\omega^{-2}$  slope that levels off at low frequencies. The time scale  $\tau^*$ , at which the spectrum levels off, is a few decades. In the model of Frankignoul et al. (1997) this time scale corresponds to the time needed for a long baroclinic Rossby wave to propagate across the ocean basin.

#### 4.2 Type II

The second type of spectra, as sketched at the bottom of Fig. 4, is characterized by a flat spectral level at high frequencies and a low-frequency spectral slope  $\omega^{-\beta_I}$  with  $\beta_I$  being positive and significantly different from zero. The spectral energy steadily increases as frequency decreases. This type of spectra is characteristic for variations in the deep tropical and subtropical oceans.

Examples of this type of spectra are given in Fig. 12, which shows the spectra of zonally averaged stream function in the intermediate (i.e. 1000 to 2000 m) Atlantic, as derived from the GFDL, ECHAM3/LSG, ECHAM1/LSG and HadCM2 integrations. The solid straight lines indicate the fitted spectral slopes. The low-frequency range, over which  $c\omega^{-\beta}$  is fitted to the spectrum, extends from two decades to five centuries. The fitted power law is close to  $\omega^{-1}$  (indicated by the lower dashed line). The spectral increase with decreasing frequency is obvious for all considered time series.

In order to identify the regions where type-II spectra are found, the low-frequency power  $\beta_I^0$  is estimated from the zonally averaged stream function. Figure 13 shows the distributions of  $\beta_I^0$  in the Atlantic, as derived from the integrations with the GFDL, ECHAM3/LSG, ECHAM1/LSG and HadCM2 models (von Storch et al. 2000). The fitting is again carried out for the frequency range extending from two decades to five centuries. At northern mid and high latitudes,  $\beta_I^0$  tends to be close to zero (light grey areas in Fig. 13), indicating that the spectra are essentially white on time scales longer than two decades. A low-frequency plateau is also found in the southern mid and high latitudes when considering a globally averaged stream function which extends to the coast of Antarctica (not shown). Thus, spectra in the mid and high latitudes resemble the type-I rather than the type-II spectrum.

The type-II spectra are only found in the deep tropical and subtropical oceans (von Storch et al. 2000). For the Atlantic, a value of  $\beta_I^0$  of about one is found at intermediate depths (dark grey areas in Fig. 13) and about two near the bottom (black areas in Fig. 13) in the GFDL, ECHAM3/LSG and ECHAM1/LSG runs. In the HadCM2 run, the values of  $\beta_I^0$  are about one at intermediate depths, but then decrease to about zero in large regions of the deeper layers.

Spectra of EOF coefficients of zonally averaged stream functions were considered in von Storch and Müller (1998). These spectra resemble the spectrum shown in the lower panel of Fig. 4. The result is a consequence of the fact that large-scale variations of the zonally averaged stream function involve anomalous circulations in the tropical and subtropical deep ocean, where type-II spectra are found.

The tendency for Type-II spectra in the deep tropical and subtropical oceans is not a special feature of the zonally averaged stream function. A similar tendency is, at least in the ECHAM1/LSG run, observed when considering zonal, meridional or vertical velocities (not shown). In general, the spectra of velocities are essentially flat in the first model layer in most parts of the ocean, as indicated by the near zero high- and low-frequency slopes. This is likely related to the fact that this layer is in direct contact with atmospheric fluxes, which are essentially white on time scales longer than a year. Note that high-frequency slopes can still be identified when using time series with finer temporal resolution. Away from the surface and in the upper few hundred

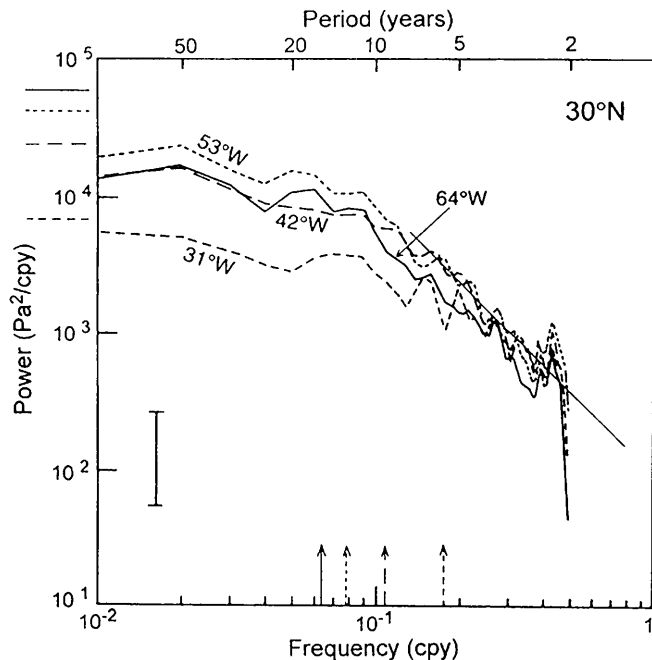
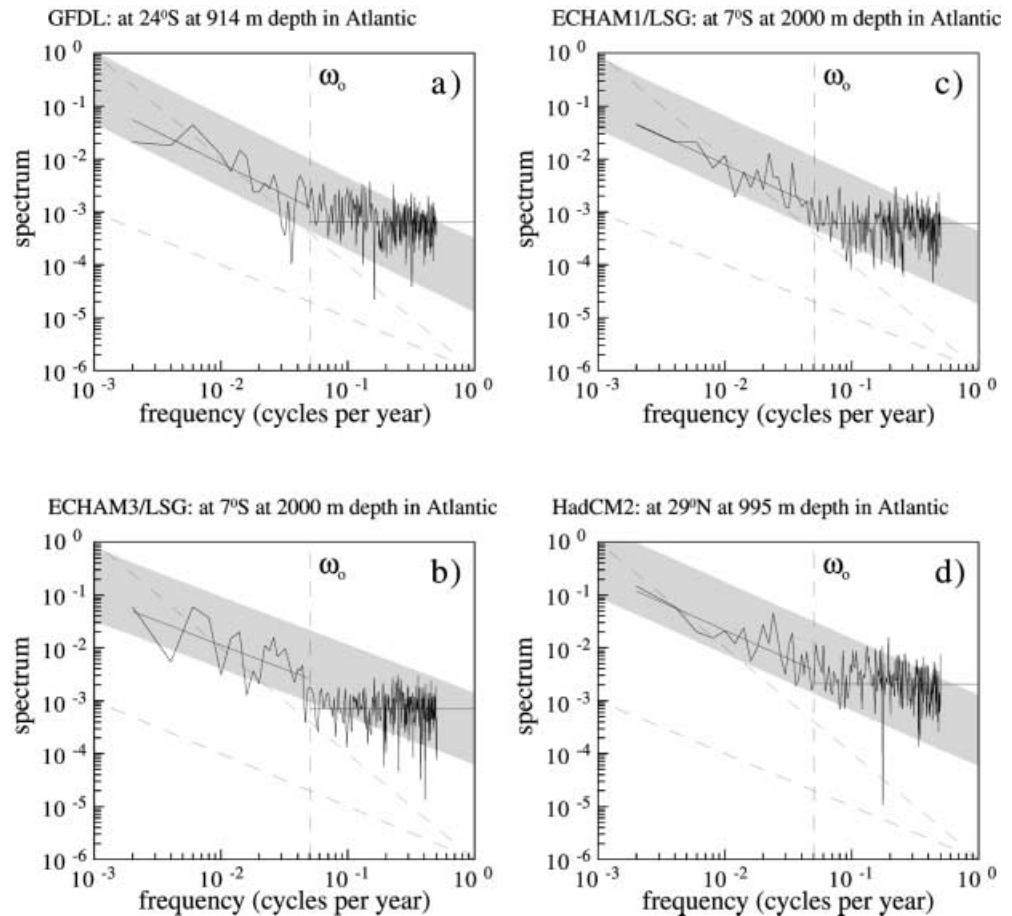


**Fig. 11** Spectra of the ECHAM1/LSG baroclinic pressure at 250 m and 30°N for various longitudes in the Atlantic. The spectra were estimated from seven independent, detrended 100-year pieces. The thin line at high frequencies is proportional to  $\omega^{-2}$ . For details, see Frankignoul et al. (1997). Frequency is in cycles per year

**Fig. 12a–d** Spectra of yearly time series at grid points in the Atlantic, where  $\beta_1^0$  is close to one. The spectra are derived from integrations with the GFDL, ECHAM3/LSG, ECHAM1/LSG and HadCM2 models. Two consecutive chunks are used to estimate the spectra. The spectral values are  $\chi^2$ -distributed with four degrees of freedom for all frequencies (except for the highest and the lowest resolvable frequencies  $\omega = 0.5$  and  $\omega = 2 \times 10^{-3}$ ). The grey band shows the 95% confidence band of the  $\chi^2$ -distribution. The solid straight line is obtained by least-square fitting  $c\omega^{-\beta}$  to the low- and high-frequency parts of the spectrum. The vertical dashed lines mark the upper bound of the low-frequency band. The two other dashed lines are proportional to  $\omega^{-1}$  and  $\omega^{-2}$ . Frequency is in cycles per year



metres of the ocean, large regions with a high-frequency  $\omega^{-2}$  slope are found in the tropical and subtropical ocean. The spectra in these regions level off at low frequencies, leading to near zero low-frequency slope. Below 450 m, the high-frequency slope starts to diminish. Below 1000 m depth, the high-frequency slope reduces to about zero and the low-frequency slope increases to about one to two in the tropical and subtropical Atlantic and in the tropical and North Pacific, indicating the emerging of type-II spectra.

This characteristic change of spectral behaviour with increasing depth in the tropical and subtropical ocean is demonstrated in Fig. 14 in terms of spectra of zonal velocity at one grid point but different depths. While the spectra in the layers between 75 to 450 m resemble type-I spectrum, the spectra at 1000 to 4000 m depth become similar to type-II spectrum. The amplitude of  $\beta_1^0$  is about one at 1000 to 3000 m depth and about two at 4000 m depth.

## 5 Discussion

### 5.1 Two different types of stochastic processes

One important difference between type-I and type-II spectra is their behaviour at low frequencies. Since a

spectrum is the Fourier transform of the corresponding auto covariance function, the low-frequency behaviour can be translated into the behaviour of the auto covariance function at large time lags. It can be shown that a spectrum, which is flat at low frequencies, is obtained when the auto covariance function decays sufficiently fast with increasing time lag. Since such a decay of the auto covariance function is indicative of a short-memory process, type-I spectra can be considered as being generated by short-memory processes, and type-II spectra, on the contrary, by long-memory processes.

ARMA (auto-regressive and moving average) processes are short-memory processes (Brockwell and Davis 1996). Long memory processes can be generated by fractional ARIMA (auto-regressive-integrated moving average) processes (Brockwell and Davis 1996, Beran 1994). While ARMA processes are widely used in climate research, fractional ARIMA processes are much less known to the climate community. In the following, fractional ARIMA processes are briefly introduced and the low-frequency behaviours of the two types of processes are discussed.

Let us first recall the definition of ARMA and ARIMA processes. Consider a process  $X_t$  with zero mean. Let  $B$  denote the backshift operator defined by  $BX_t = X_{t-1}$ . Differences can then be expressed in terms of the backshift operator as  $X_t - X_{t-1} = (1 - B)X_t$ ,

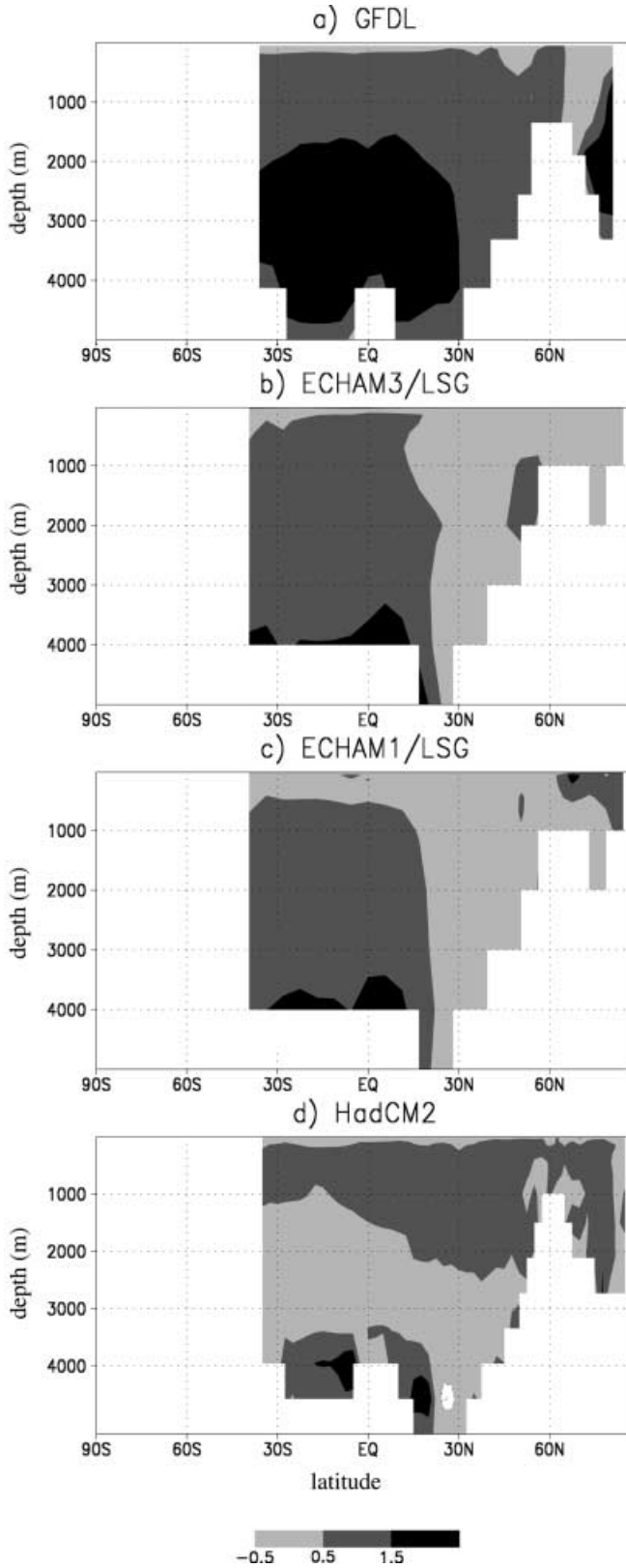


**Fig. 13a–d** Low-frequency spectral power  $\beta_l^0$  of yearly zonally averaged stream functions in the Atlantic, obtained from the GFDL, ECHAM3/LSG, ECHAM1/LSG and HadCM2 millennium integrations. The *black, dark and light grey areas* indicate the areas where values of the spectral power  $\beta_l^0$  are close to two, one and zero, respectively

$(X_t - X_{t-1}) - (X_{t-1} - X_{t-2}) = (1 - B)^2 X_t$ . The auto-regressive operator can be expressed as the polynomial  $\phi(B) = 1 - \sum_{i=1}^p \alpha_i B^i$ , and the moving average operator by  $\psi(B) = 1 + \sum_{j=1}^q \mu_j B^j$ , where  $p$  and  $q$  are integers, and  $\alpha_i$  and  $\mu_j$  are constants (parameters) such that  $\alpha_p \neq 0$  and  $\mu_q \neq 0$ .  $X_t$  is said to be an ARMA( $p, q$ ) process of order ( $p, q$ ), if

$$\phi(B)X_t = \psi(B)Z_t \quad (2)$$

where  $Z_t$  is a white noise process. An auto-regressive process AR( $p$ ) is an ARMA( $p, 0$ ) process. If instead Eq. (2) holds for the  $d$ th difference  $(1 - B)^d X_t$  with  $d$  being a non-negative integer, i.e.

$$\phi(B)(1 - B)^d X_t = \psi(B)Z_t \quad (3)$$

then  $X_t$  is called an ARIMA( $p, d, q$ ) process of order ( $p, d, q$ ). Equation (3) reduces to Eq. (2) when  $d = 0$ . Equation (3) can be generalized in a natural way by allowing  $d$  to be any real value. For  $-1/2 < d < 1/2$ ,  $X_t$  is called a fractional ARIMA process. Thus, a fractional ARIMA process is a natural extension of an ARIMA and ARMA process.

Note that an ARIMA process with a positive integer  $d$  is not stationary, whereas a fractional ARIMA process with  $-1/2 < d < 1/2$  can be (depending on the process parameters) stationary. A non-stationary process with  $d > 1/2$  can be reduced to the case  $-1/2 < d < 1/2$  by taking appropriate differences. Non-stationarity is often related to a trend. Such a trend may occur in the deep ocean, even though von Storch et al. (2000) showed that similar low-frequency spectral shapes are obtained when the first few hundred years (which are affected by initial drifts) are removed from the time series. Nevertheless, the effect of trends cannot be completely ruled out.

Apart from trends, there is another feature, namely the spectral value at frequency  $\omega = 0$ , which distinguishes an ARMA process from an fractional ARIMA process. The value of  $\Gamma(0)$  is bounded for an ARMA process, but infinite for an ARIMA( $p, d, q$ ) process with  $d > 0$ . Since the spectrum is a continuous function,  $\Gamma(0)$  has to be steadily approached as  $\omega \rightarrow 0$ . Different values of  $\lim_{\omega \rightarrow 0} \Gamma(\omega)$  must therefore be related to different low frequency behaviours.

The spectrum of an ARMA process is given by Brockwell and Davis (1996)

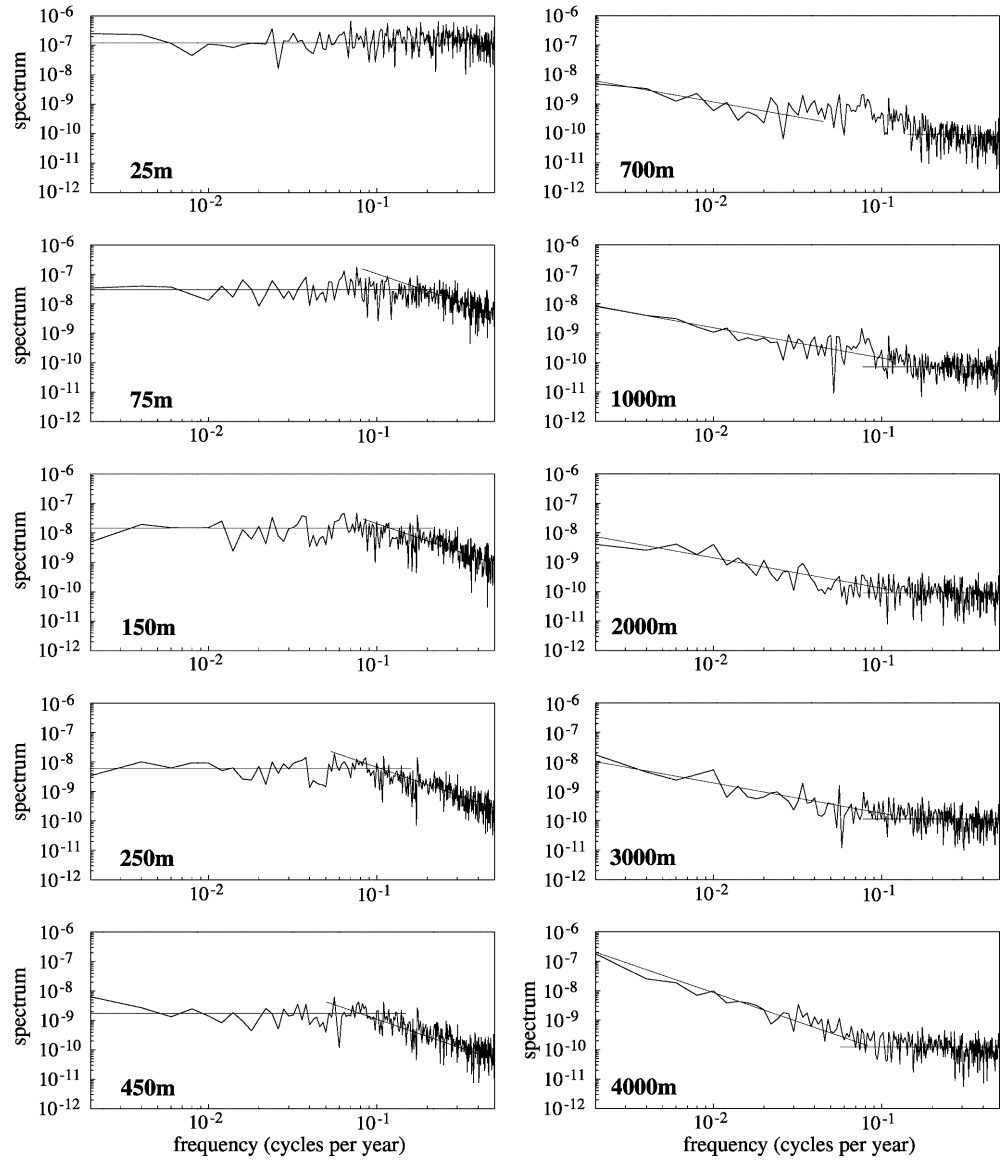
$$\Gamma_{ARMA}(\lambda) = \frac{\sigma_z^2 |\psi(e^{i\lambda})|^2}{2\pi |\phi(e^{i\lambda})|^2} \quad (4)$$

where  $\lambda$  is the angular frequency with  $\lambda = 2\pi\omega$  and  $\sigma_z^2$  is the variance of the white noise forcing of the process. As  $\lambda \rightarrow 0$ ,  $\Gamma_{ARMA}(\lambda)$  approaches

$$\Gamma_{ARMA}(0) = \frac{\sigma_z^2 |\psi(1)|^2}{2\pi |\phi(1)|^2} \quad (5)$$

$\Gamma_{ARMA}(0)$  equals the integral of the auto covariance function and has a finite value. For a white noise process AR(0),  $\Gamma_{ARMA}(0)$  equals the variance of the noise. For an AR(1) process,  $\Gamma_{ARMA}(0)$  is given in the last line of Eq. (1).

**Fig. 14** Spectra of yearly zonal velocity at (39°W, 4°N) at various depths. The depths, indicated in the lower left corner of each diagram, correspond to the depths of the vertical layers in the LSG model. The spectra are estimated from two consecutive chunks. The spectral shape changes with increasing depth. In the upper 450 m, the spectra resemble type-I spectra. The straight lines are parallel to  $\omega^0$  and  $\omega^{-2}$ . Below 450 m, the spectra resemble type-II spectra. The spectra are flat at high frequencies, but increase with decreasing frequency at the rate of  $\omega^{-1}$  at 700 to 3000 m depth and at the rate of  $\omega^{-2}$  at 4000 m depth. Frequency is in cycles per year



The spectrum of an ARIMA or a fractional ARIMA process follows directly from Eq. (4) (see e.g. Beran 1994),

$$\Gamma_{ARIMA}(\lambda) = |1 - e^{i\lambda}|^{-2d} \Gamma_{ARMA}(\lambda) \quad (6)$$

where the factor  $|1 - e^{i\lambda}|^{-2d}$  originates from the operator  $(1 - B)^d$  in Eq. (3). Since  $|1 - e^{i\lambda}| = 2 \sin(\lambda/2)$  and  $\lim_{\lambda \rightarrow 0} \frac{1}{\lambda} (2 \sin(\lambda/2)) = 1$ , the behaviour of the spectrum (6) at low frequencies with  $\lambda \rightarrow 0$  is given by

$$\Gamma_{ARIMA}(\lambda) = \Gamma_{ARMA}(0) |\lambda|^{-2d} \quad (7)$$

For  $d < 0$ ,  $\Gamma_{ARIMA}(0) = 0$ . For  $d > 0$ ,  $\Gamma_{ARIMA}(0)$  is infinite, the spectrum has a singularity at  $\lambda = 0$ .

Equations (5) and (7) show that, as  $\lambda \rightarrow 0$ , the spectral behaviour of an ARMA process differs significantly from that of a fractional ARIMA process with  $0 < d < 1/2$ . As  $\lambda$  approaches zero,  $\Gamma_{ARMA}(\lambda)$  approaches a bounded value  $\Gamma_{ARMA}(0)$ , but  $\Gamma_{ARIMA}(\lambda)$  becomes infinite.

The millennium integrations are certainly too short for considering the situation  $\omega \rightarrow 0$ . However, there is an integration over 15 000 years obtained with the simplified coupled ECBILT model (Opsteegh et al. 1997; Selten et al. 1997). The oceanic component of this coupled model is a simplified version of the GFDL ocean GCM with flat bottom. The atmospheric model is a global quasi-geostrophic model. Figure 15 shows the time series and the spectrum of the maximum stream function in the Atlantic, which characterizes the northward mass transport of the Atlantic overturning circulation. A period of 6000 years of the 15 000-year integration, which does not obtain obvious trends, are considered. Since two chunks are used to estimate the spectrum, the longest resolvable time scale increases from 500 years for the millennium runs to 3000 years for the ECBILT integration. The ECBILT model produces pronounced variations on decadal time scales. But over the time-scale range extending from a few decades to

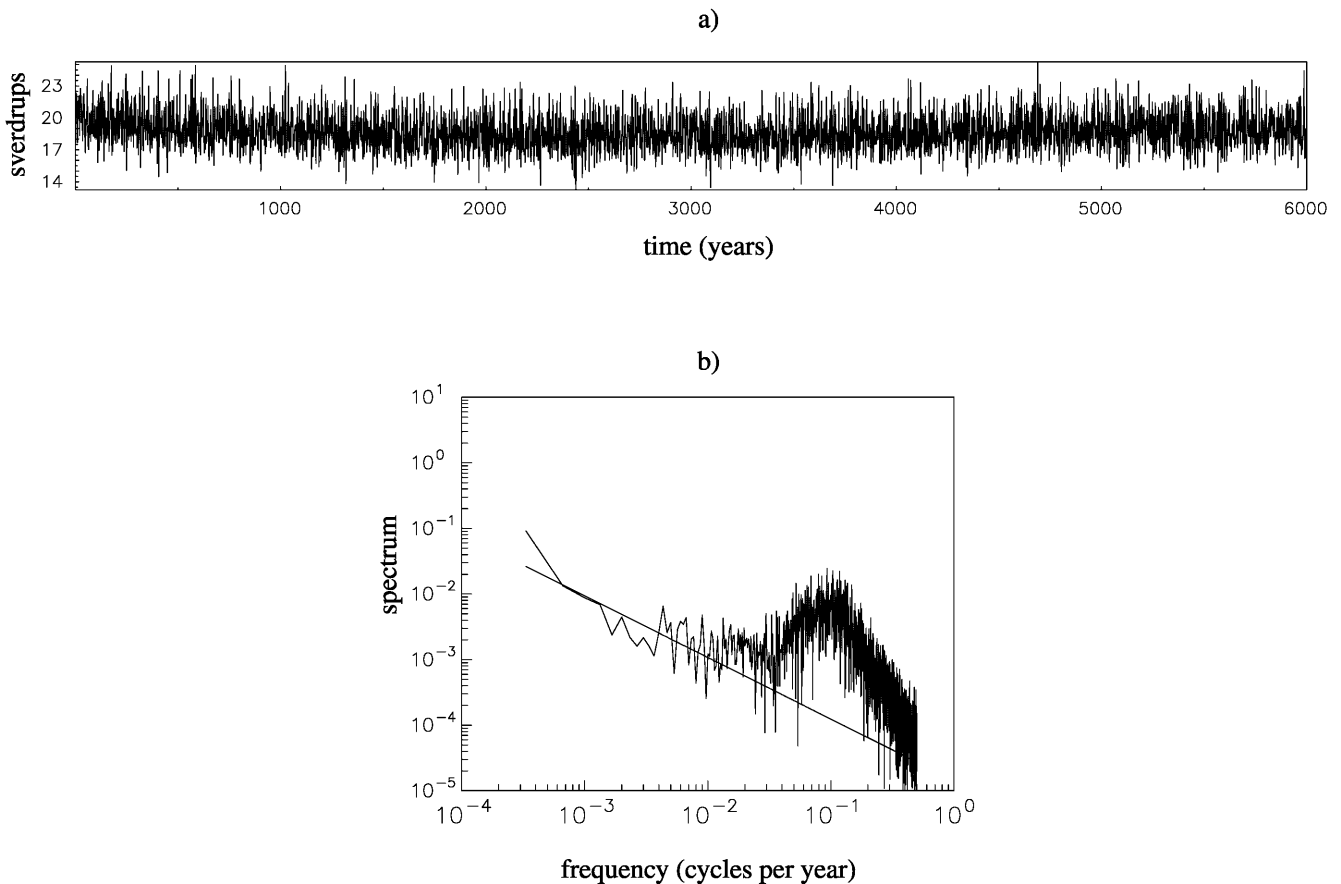


**Fig. 15a, b** Time series and spectrum of the maximum of yearly zonally averaged stream function in the Atlantic, obtained from a 15 000-year integration with the simplified coupled ECBILT model. The

3000 years, the spectrum can be approximately described by the power law  $\omega^{-1}$ . Figure 15b supports the tendency of the steady increase of spectral energy with decreasing frequency found in the coupled GCM integrations.

## 5.2 Why does the type-I spectrum disappear in the deep ocean?

In order to answer this question, it is natural to consider properties which exist in the atmosphere and the upper ocean, but are almost absent in the deep ocean. Fluctuations induced by atmospheric synoptic dynamics are an obvious candidate which satisfies this condition. They are omnipresent in the atmosphere. They can directly affect the upper ocean through surface fluxes. At high latitudes, they can penetrate to great depth through deep convection. In the tropics and subtropics, the stratification is more stable than in the high-latitude regions, and the penetration can become difficult.

The importance of short-term fluctuations in generating type-I spectra is further supported by the concept of stochastic climate models (Hasselmann 1976). Consider a variable  $x$  governed by the equation

straight line in **b** marks the fitted low-frequency power law, which is close to  $\omega^{-1}$ . Frequency is in cycles per year

$$\frac{dx}{dt} = f \quad (8)$$

where  $f$  is generally a non-linear function of  $x$  and other variables. The spectral representation of Eq. (8) is

$$\Gamma_x(\omega) = \frac{\Gamma_f(\omega)}{2\pi} \omega^{-2} \quad (9)$$

The  $\omega^{-2}$  results from the differential operator in Eq. (8). If  $f$  is not a white noise process,  $\Gamma_f(\omega)$  will be a function of  $\omega$ . The spectral slope of  $\Gamma_x(\omega)$  will be generally different from  $\omega^{-2}$ . On the other hand, short-term fluctuations can be represented by white noise. If  $f$  is dominated by such fluctuations,  $\Gamma_f(\omega)$  will be essentially independent of  $\omega$ , and a  $\omega^{-2}$  slope will emerge. The concept of the stochastic climate model suggests that at low frequencies, negative feedbacks must be at work. These feedbacks will force the spectrum to level off at low frequencies.

In general, Eq. (9) suggests that a high-frequency  $\omega^{-2}$  slope is indicative of the involvement of white noise forcing. The type-I spectrum describes the spectral properties of atmospheric and oceanic variables which are exposed to fluctuations, whereas the type-II spectrum is characteristic for deep ocean areas which are shielded from fluctuations.

Accepting that type-I spectra are indicative of the presence of short-term fluctuations, the results of Sect. 4.2 suggest how fluctuating fluxes at the surface penetrate to the deep ocean in the ECHAM1/LSG integration. The deepest penetration occurs in the high-latitude parts of the ocean, where the spectra in the deep layers are comparable to that shown in the upper panel of Fig. 4. The only exception is the southern Atlantic in the ECHAM1/LSG run where a non-zero low-frequency slope is already apparent in the upper ocean. The weakest penetration occurs in the tropical and subtropical Pacific and in the tropical and subtropical Atlantic, where the type-I spectra cannot be found in the deep layers.

### 5.3 Is the type-II spectrum real?

There are two reasons suggesting that the type-II spectra are a model-specific phenomenon. First, following the discussion of Sect. 2.1, the ocean models considered are coarse-resolution models and do not produce oceanic eddies. Since type-I spectra suggest the dominance of short-term fluctuations in generating the variations, and such fluctuations are not present in the interior of the ocean, which is shielded from the fluctuating fluxes at the surface, the disappearance of type-I spectra can be a consequence of the lack of internal noise. It is beyond the scope of this study to provide a rigorous consideration of this possibility. Nevertheless, the possibility indicates potential problems when using coarse-resolution ocean GCMs to study variability in the deep ocean, and underline the need for eddy resolving ocean GCMs when studying long-term oceanic variations.

The second reason relates to the dissipation processes in the model. The type-II spectra imply infinite spectral values at the origin. Without having a physical explanation for such a spectral behaviour, one would first assume that the steady increase of spectral energy with decreasing frequency is indicative of a lack or an underestimation of dissipation processes in the model. Since it is not clear how the ocean dissipates the energy imposed at the surface, it is difficult to verify the dissipation processes in the models, and hence to assess the realism of the type-II spectra.

We can certainly not rule out the possibility that the spectra in the deep tropical and subtropical ocean will eventually level off, but at much lower frequencies. In order to clarify this, much longer integrations are required. In any case, there is a long way to go to achieve a complete understanding of long-term variations in the deep ocean. Due to the lack of observations, progress can only be made in terms of numerical integrations.

## 6 Conclusions

This work studies the spectral behaviour of the variability in millennium integrations of coupled atmosphere-ocean GCMs. Two distinctly different types of

spectra are identified. The type-I spectra, characterized by a spectral plateau at low frequencies and a  $\omega^{-2}$  slope at high frequencies, are obtained for many atmospheric variables and variables representing predominantly the upper ocean and the high-latitude part of the deep ocean. The time scale  $\tau^*$ , at which the spectrum levels off, is no longer than one year in the atmosphere, about 7 to 8 years for the NINO3 SST, and about a few decades for the oceanic baroclinic Rossby waves. The type-II spectra are characterized by a low-frequency slope  $\omega^{-\beta_f^0}$  with  $\beta_f^0 > 0$  and are indicative of a steady spectral increase with decreasing frequency. They are observed in the deep tropical and subtropical oceans of the GFDL, ECHAM3/LSG and ECHAM1/LSG runs. The HadCM2 model produces type-II spectra only in the tropical and subtropical Atlantic at intermediate depths.

Following the concept of stochastic climate models, the high-frequency  $\omega^{-2}$  slope indicates the importance of short-term fluctuations in generating climate variations. Such fluctuations are omnipresent in the atmosphere, but do not exist in the interior of the ocean which is shielded from the surface forcing. Nevertheless, since surface fluxes can penetrate into the ocean, in particular at high latitudes where deep convection occurs, type-I spectra are also found in the upper ocean and the high-latitude part of the deep ocean. In the tropical and subtropical oceans, where the mean stratification is stable and penetration becomes difficult, a new type of spectra emerges. The variables in these regions can be considered as being generated by fractional ARIMA processes. Accepting the dominant role of noise in generating type-I spectra, the distribution of the two spectral types indicates how fluctuating fluxes, which are imposed at the surface, penetrate and affect variations in the deep ocean. In the ECHAM1/LSG model, this penetration is most pronounced in the North Atlantic and in the South Pacific and Southern Ocean.

The realism of type-II spectra is questionable for two reasons. First, since the ocean GCMs used do not resolve oceanic eddies, the lack of fluctuations in the deep ocean can be a specific feature of the coarse-resolution models. Secondly, it is not clear to what extent the present-day coupled GCMs realistically simulate the dissipation processes in the deep ocean. The lack or underestimation of such processes may be responsible for the observed steady increase of spectral energy with decreasing time scales in the deep oceans.

**Acknowledgements** The authors are grateful to Reindert Haarsma for providing the KNMI integration.

## References

- Beran J (1994) Statistics for long-memory processes. Chapman and Hall, New York, pp 315
- Brockwell PJ, Davis RA (1996) Time series: theory and methods. Springer, New York Berlin Heidelberg, pp 577
- Cubasch U, Hasselmann K, Höck H, Maier-Reimer E, Mikolajewicz U, Santer BD, Sausen R (1992) Time-dependent

- greenhouse warming computations with a coupled ocean-atmosphere model. *Clim Dyn* 8: 55–69
- Frankignoul C, Müller P, Zorita E (1997) A simple model of the decadal response of the ocean to stochastic wind forcing. *J Phys Oceanogr* 27: 1533–1546
- Hasselmann K (1976) Stochastic climate models. Part I: theory. *Tellus* 28: 473–485
- Manabe S, Stouffer RJ (1996) Low frequency variability of surface air temperature in a 1000 year integration of a coupled ocean-atmosphere model. *J Clim* 9: 376–393
- Manabe S, Stouffer RJ, Spelman MJ, Bryan K (1991) Transient responses of a coupled ocean-atmosphere model to gradual changes of atmospheric CO<sub>2</sub>. Part I: annual mean response. *J Clim* 4: 785–818
- Opsteegh JD, Haarsma RJ, Selten FM (1998) ECBILT; a dynamic alternative to mixed boundary conditions in ocean models. *Tellus* 50A: 348–367
- Roemmich DH, Wunsch C (1985) Two transatlantic sections: meridional circulation and heat flux in the subtropical North Atlantic Ocean. *Deep-Sea Res* 32: 619–664
- Sausen R, Barthels K, Hasselmann K (1988) Coupled ocean-atmosphere models with flux correction. *Clim Dyn* 2: 154–163
- Selten FM, Haarsma RJ, Opsteegh JD (1997) On the mechanism of North Atlantic decadal variability. KNMI reprint 97-31, Royal Netherlands Meteorological Institute, De Bilt, The Netherlands
- Stouffer RJ, Dixon KW (1998) Initialization of coupled models for use in climate studies: a review. In: *Research activities in atmospheric and oceanic Modelling*, Rep 27, WMO/TD-No. 865, WMO, Geneva, Switzerland
- Stouffer RJ, Hegerl G, Tett SFB (2000) A comparison of surface air temperature variability in three 1000-yr coupled ocean-atmosphere model integrations. *J Clim* 13: 513–537
- Tett SFB, Johns TC, Mitchell JFB (1997) Global and regional variability in a coupled AOGCM. *Clim Dyn* 13: 303–323
- Timmermann A, Latif M (1999) Modes of climate variability as simulated by the coupled atmosphere-ocean model ECHAM3/LSG, Part I: ENSO-like climate variability. *Clim Dyn* (in press)
- von Storch H, Zwiers FW (1999) *Statistical analysis in climate research*. Cambridge University Press, Cambridge, UK, pp 494
- von Storch J-S (1994) Interdecadal variability in a global coupled model. *Tellus* 46A: 419–432
- von Storch J-S (1999) On the reddest atmospheric modes and the forcings of the spectra of these modes: a description. *J Atmos Sci* 56: 1614–1626
- von Storch J-S, Müller P (1998) Decadal variability in millennium integrations with coupled atmosphere-ocean general circulation models. In: Holloway G, Müller P, Henderson D (eds). *Biotic impacts of extratropical climate variability in the Pacific*. Proce Aha Huliko'a Hawaiian Winter Workshop, School of Ocean and Earth Science and Technology, Special Publication
- von Storch J-S, Kharin V, Cubasch U, Hegerl GC, Schriever D, von Storch H, Zorita E (1997) A description of a 1260-year control integration with the coupled ECHAM1/LSG general circulation model. *J Clim* 10: 1526–1544
- von Storch J-S, Müller P, Stouffer RJ, Voss R, Tett SFB (2000) Variability of deep-ocean mass transport: spectral shapes and spatial scales. *J Clim* 13: 1916–1935
- Voss R (1996) Entwicklung eines Kopplungsverfahrens zur Reduzierung der Rechenzeit von Atmosphäre-Ozean Modellen. *Examensarbeit* 38. DKRZ, Hamburg, Germany
- Voss R, Sausen R, Cubasch U (1998) Periodically synchronously coupled integrations with the atmosphere-ocean general circulation model ECHAM3/LSG. *Clim Dyn* 14: 249–266
- Xu J-S, von Storch U, van Loon H (1990) The performance of four spectral GCMs in the Southern Hemisphere: the January and July climatology and the semiannual wave. *J Clim* 3: 53–70